Peer-reviewed version available at J. Imaging 2019, 5, 12; doi:10.3390/jimaging5010012

Article

Semi-automatic Algorithms for Estimation and Tracking of AP-diameter of the IVC in Ultrasound Images

Ebrahim Karami [1,*], Mohamed Shehata [1] Andrew Smith [2]

[1] Affiliation 1; Department of Engineering and Applied Sciences, Memorial University, Canada, {ekarami,mshehata}@mun.ca
[2] Affiliation 2; Faculty of Medicine, Memorial University, Canada, andrew.smith@med.mun.ca
* Correspondence: ekarami@mun.ca; Tel.: +1-709-740-6129

Version October 30, 2018 submitted to

Abstract: Medical research has suggested that the anterior-posterior (AP)-diameter of the inferior vena cava (IVC) and its associated temporal variation as imaged by bedside ultrasound is useful in guiding fluid resuscitation of the critically-ill patients. This paper develops semi-automatic active ellipse and rectangle algorithms for measurement and tracking of the AP-diameter. The proposed algorithms are compared with an expert manual measurement and the previous work based on active circle model. It is shown that regardless of the shape of the IVC, the rectangle model always outperforms the two other models and performs very close to manual measurement.

Keywords: Inferior vena cava (IVC); ultrasound imaging; anterior posterior (AP) diameter; active ellipse; active rectangle; volume status.

1. Introduction

Estimation and monitoring of relative changes in circulating blood volume is critically important for several medical conditions including hemorrhage from trauma, stomach ulcers, blood vessel rupture, septic shock, and volume overload in the setting of congestive heart failure. Fast and accurate monitoring of circulating blood volume is a challenging task as excessive or insufficient fluid administration increases patient morbidity and mortality[1,2]. Clinical research has suggested that the variations in the anterior-posterior (AP) diameter of inferior vena cava (IVC) is correlated with patient's volume status [3–5]. Clinically, the AP-diameter is manually estimated from portable ultrasound imagery which is a tedious and time-consuming task in the setting of poor image quality. Furthermore, artifacts such as shadowing and speckle noise frequently result in indistinct edges and gaps in the vessel walls reducing the accuracy of manual measurement[6,7].

Speckle noise present in ultrasound imagery is theoretically considered to be a Rayleigh distributed multiplicative noise [8] as the envelop of the ultrasound wave reflected from each tissue has a Rayleigh distribution. Hence, Rayleigh mixture models have been proposed as a solution for ultrasound image segmentation [9,10]. However, it has been shown that due to the scattering population and signal processing, the speckle distribution deviates from Rayleigh[11]. In [12], authors proposed a fast algorithm based on optical flow for tracking of the speckles in ultrasound images. This approach fails when the speckle structure is rapidly deformed.

Active contours (ACs) are widely used for segmentation of ultrasound images [13–17]. ACs convert the problem of image segmentation into a minimization of an energy functional with their performance frequently dependent on a manually-defined initialization contour. In order to avoid local minima, the initiating contour needs to be as close as possible to the actual contour. ACs can be combined with other segmentation algorithms as a coarse-to-fine strategy to reduce the impact of the initial contour on segmentation error [18,19]. Researchers have addressed the challenge of IVC segmentation using this strategy by using template matching method as the coarse segmentation and AC as the fine-tuning (TMAC) [20]. Unfortunately, this approach fails when the IVC undergoes large frame-to-frame

variations commonly present on portable machines with lower frame rates (e.g. 30 frames-per-second). Additionally, ACs continue to perform poorly in the context of fuzzy or unclear boundaries as is commonly the case for the IVC.

Given that the cross-section of the IVC is largely convex, the IVC contour can be represented in polar coordinates and consequently, polar active contours appear as a promising solution for IVC segmentation [21]. In [22], a polar AC model based on the third centralized moment (M3) was proposed for segmentation of IVC images. Unfortunately, M3 algorithms roughly estimates the cross-sectional area (CSA) of the IVC and fails with poor quality images.

Clinically the CSA of the IVC is an optimal approach to accurately assess a patient's volume status, but all existing approaches fail to accurately estimate the CSA. Hence, clinicians instead of the the whole CSA of the IVC, measure its AP-diameter. In [23], AP-diameter was modeled as the diameter of a circle fitted inside IVC. This approach, although provides good results, it deviates with the clinical definition of AP-diameter. Clinicians measures the AP-diameter as the largest vertical diameter in the IVC and obviously, if the CSA of the IVC is deviated from the horizontal angle, the circle diameter slightly defers from the clinically measure AP-diameter.

In this paper, we propose two algorithms based on ellipse and rectangle models. The height of a thin rectangle fitted inside the IVC can efficiently model its clinically measured AP-diameter. We also develop another algorithm based on ellipse fitting just for comparison purpose.

The remainder of this paper is organized as follows - Section 2 discusses the background and related work. The proposed active rectangle and active ellipse algorithms are presented in Section 3 while experimental results are in Section 4, the results are discussed in Section 5 and the paper is concluded in Section 6.

2. Background and Related Work

In [23], authors showed that the AP-diameter of the IVC can be accurately modeled with the diameter of a circle fitted in inside the IVC. The active circle algorithm proposed in [23] is based on the following evolution functional:

$$E = \alpha(u-v)(2I-u-v), \tag{1}$$

where u and v are the mean of the intensities for the pixels inside and outside the contour, respectively, and I is the intensity of the pixels on the contour. This functional is used to evolve the parameters of the circle, i.e., R as the circle radius and (x_c, y_c) as its center coordinates. For this, the circle is sampled at K points with polar angles $\theta_k = \frac{2k\pi}{N}$, $k = 0, 1, ..., K-1$, where the normal vector and the Cartesian coordinates corresponding to the kth sampled point are denoted as

$$\vec{n}_k = [\cos(\theta_k), \sin(\theta_k)]^T, \tag{2}$$

and

$$[x_k, y_k]^T = [x_c, y_c]^T + R\vec{n}_k, \tag{3}$$

respectively. The evolution functional generates forces

$$f_k = \alpha(u-v)(2I_k-u-v) \tag{4}$$

along the normal vectors. The forces shift the sampled contour points to new positions governed by

$$[\tilde{x}_k, \tilde{x}_k] = [x_c, y_c]^T + (R+f_k)\vec{n}_k. \tag{5}$$

where f_k is the value of the evolution functional at kth contour point. It is shown that the average evolution functional approaches zero when the contour points are on the IVC boundary. In active circle algorithm, the center of the circle is evolved as

$$[\tilde{x}_c, \tilde{y}_c] = [x_c, y_c] + \frac{1}{K}\sum_{k=0}^{K-1} f_k \vec{n}_k, \tag{6}$$

where $[x_c, y_c]$ and $[\tilde{x}_c, \tilde{y}_c]$ the center coordinates of the circle before and after evolution, respectively, and f_k is the evolution force for the kth contour points obtained from 1, and $\vec{n}_k$ is its corresponding normal vector that can be obtained as

$$\vec{n}_k = [\cos(\theta_k), \sin(\theta_k)]^T, \tag{7}$$

Eq. (6) indicates that for a given set of forces the circle center is simply shifted by the average of the force vectors $f_k \vec{n}_k$.
The center of the circle is evolved as

$$\tilde{R} = R + \frac{1}{K}\sum_{k=0}^{K-1} f_k. \tag{8}$$

where R and $\tilde{R}$ is the radius of the circle before and after evolution, respectively. This indicates that for a given set of forces, the circle radius is evolved with the average of the force values f_k.

3. Proposed Algorithms

In this section, we develop active ellipse and rectangle models based on the evolution functional proposed in [23].

3.1. Active Ellipse Model

In [23], authors showed that the active circle algorithm estimates the IVC AP-diameter much more accurate than the star-Kalman algorithm in [24] which is based on ellipse fitting. But does this indicate that a circular model can estimate the AP-diameter more accurate than an elliptical model? To answer this question, we develop an active ellipse algorithm based on the same evolutional functional as the one in the active circle algorithm.
In general case, during the evolution, the kth contour point is evolved as

$$[\tilde{x}_k, \tilde{x}_k] = [x_k, y_k]^T + f_k \vec{n}_k. \tag{9}$$

To fit an ellipse to these K evolved points, we use the following conic equation.

$$ax^2 + bxy + cy^2 + d * x + e * y = 1, \tag{10}$$

where x and y are the coordinate of the points on the conic, a, b, c, d, and e are the conic parameters. Note that with an ellipse, the values of a and b must be positive. With K points with coordinates $[\tilde{x}_k, \tilde{x}_k]$, the best ellipse is fitted by minimizing the following cost function.

$$C = \sum_{k=1}^{K} (a\tilde{x}_k^2 + b\tilde{x}_k\tilde{y}_k + c\tilde{y}_k^2 + d\tilde{x}_k + e\tilde{y}_k - 1)^2 \tag{11}$$

Eq. (11) can be rewritten in matrix form

$$C(A) = A^T X^T X A + 2\mathbf{1}_K^T X A + K, \tag{12}$$

where the vector of conic parameters defined as $A = [a,b,c,d,e]^T$, X is a matrix with $[\tilde{x}_k^2, \tilde{x}_k, \tilde{y}_k, \tilde{y}_k^2, \tilde{x}_k, \tilde{y}_k]$ as its kth row, $\mathbf{1}_K$ is $K \times 1$ all-one vector, and superscript T is the transpose operator. After setting the gradient $C(A)$ to zero, the vector A is obtained as

$$\hat{A} = -\mathbf{1}_K^T X (X^T X)^{-1}. \tag{13}$$

The active ellipse algorithm is summarized in table 1.
Fig. 1 shows the ellipse evolution versus the number of iterations for a sample IVC frame.

Active ellipse algorithm for estimation and tracking of the IVC AP-diameter

Input: An IVC video and parameter $\alpha = 10^{-4}$.
- Read one frame from the input video.
- If it is the first frame, select one point inside the IVC by a mouse click. This point is assumed as the initial value of the ellipse center. The initial ellipse is created as circle centered at this point and initial radius R=8 pixels.
-
- Compute the forces for the points on each side of the rectangle using (4).
- Update the ellipse parameters using (13).
- Repeat the last two steps until a convergence is achieved. We assume the algorithm has reached the convergence when the maximum of the change in the elements of the A is less than 10^{-4}, i.e., when $max(|\hat{A}_n - \hat{A_{n-1}}|)$, where max is the element-wise maximum, and $\hat{A}_n$ is the vector A estimated at nth iteration.
- Return to the first step for the next frame.

Preprints (www.preprints.org) | NOT PEER-REVIEWED | Posted: 30 October 2018 doi:10.20944/preprints201810.0704.v1

Peer-reviewed version available at J. Imaging 2019, 5, 12; doi:10.3390/jimaging5010012

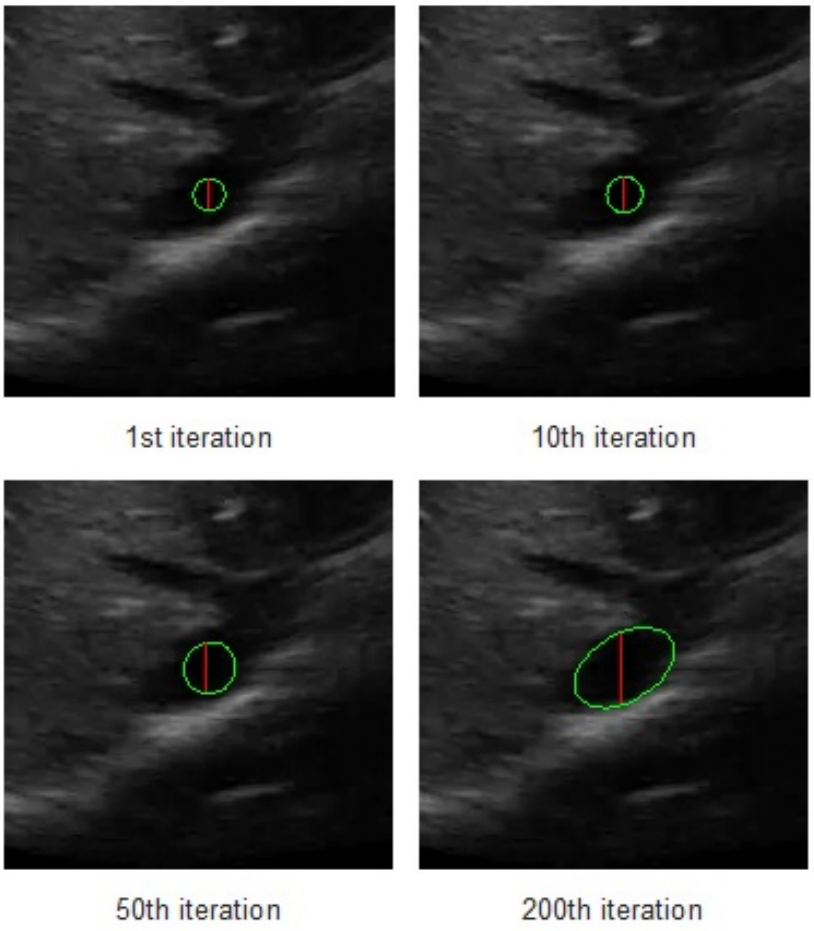

Figure 1. The rectangle evolution versus number of iterations.

3.2. Active Rectangle Model

The intuition to use a rectangular model is that the AP-diameter is clinically defined as the largest vertical diameter of the IVC contour which may practically deviate from the actual diameter of an circle or even an ellipse. The AP-diameter can be modeled as the height of a vertical thin rectangle. As a start point, we assume that the fitted rectangle has a fix width w=3pixels and the only parameters that have to be modified are the center and the height of the rectangle. With the forces defined as (4), either of the upper and lower sides of the rectangle move with the average of the forces applied on that side. Hence, the center of the rectangle is moved as

$$\tilde{x_c} = x_c + \frac{1}{K_l}\sum p \in P_l f_p - \frac{1}{K_r}\sum p \in P_r f_p, \tag{14}$$

$$\tilde{y_c} = y_c + \frac{1}{K_u}\sum p \in P_u f_p - \frac{1}{K_b}\sum p \in P_b f_p, \tag{15}$$

where P_l, P_r, P_u, and P_b are the subsets of the contour points on the left, right, upper, and lower sides of the rectangle, respectively, and K_l, K_r, K_u, and K_b are the number of points in each of these sets. Similary the height of the rectangle is evolved as

$$\tilde{h} = h + \frac{1}{K_u}\sum p \in P_u f_p + \frac{1}{K_b}\sum p \in P_b f_p. \tag{16}$$

Although a thin rectangle model accurately models the clinically measured AP-diameter, it might be lost if parts of the IVC boundaries are missing as the IVC edges are not detected and hence, the

Preprints (www.preprints.org) | NOT PEER-REVIEWED | Posted: 30 October 2018 doi:10.20944/preprints201810.0704.v1

Peer-reviewed version available at J. Imaging 2019, 5, 12; doi:10.3390/jimaging5010012

algorithm may diverge. To combat this problem, we modify the active rectangle algorithm by starting with a rectangle with a much larger width as w=15 pixels. This rectangle is gradually narrowed to its final width, i.e., w=3 pixels which is narrow enough to model the AP-diameter. The active rectangle algorithm is summarized as

Active rectangle algorithm for estimation and tracking of the IVC AP-diameter

Input: An IVC video and parameter $\alpha = 10^{-4}$.
- Read one frame from the input video.
- If it is the first frame, select one point inside the IVC by a mouse click. This point is assumed as the initial value of the rectangle center.
- Create a rectangle with initial width $w = 15$ and height h=4 pixels.
- Compute the forces for the points on each side of the rectangle using (4).
- Update the height and center of the IVC using equations (14), (15), and (16) and shrink the rectangle width with factor $0.2^{1/N}$ where N is the number of iterations. In this paper, we set N=200 iterations.
- Repeat the last two steps for N=200 iterations.
- Return to the first step for the next frame.

Fig. 2 shows the rectangle evolution versus number of iterations for the IVC image as in Fig. 1. By comparison of Figs. 1 and 2, one can see the active rectangle algorithm not only converges faster but also more accurately estimates the AP-diameter than the active ellipse algorithm.

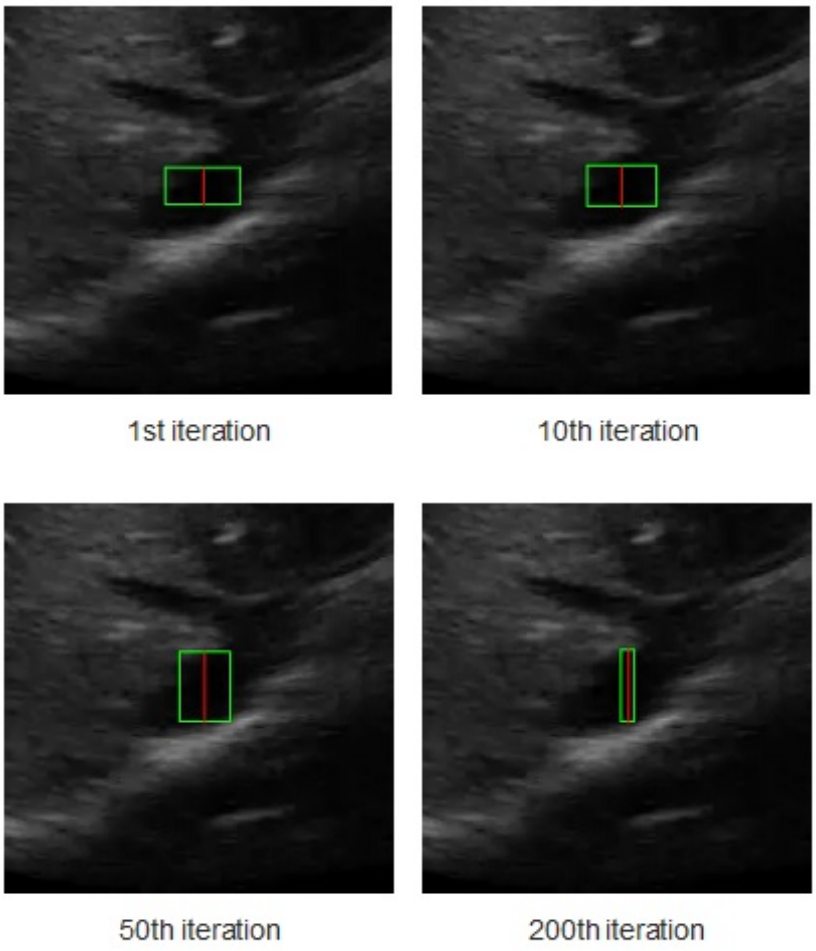

Figure 2. The rectangle evolution versus number of iterations.

4. Results

The experimental data was collected from eight young healthy male subjects. The study protocol was reviewed and approved by the Health Research Ethics Authority. The IVC was imaged in the transverse plane using a portable ultrasound (M-Turbo, Sonosite-FujiFilm) with a phased-array probe (1-5 Mhz). Each video has a frame rate of 30 fps, scan depth of 19cm, and a duration of 15 seconds (450 frames/clip). Fig. 3 depicts the first frame of all eight subjects. In Fig. 3, we can see that an IVC image can have different shapes and qualities. For instance, in the clip no. (1), although part of the image is shadowed, but the IVC edges are almost visible. The IVC videos for the clips no. (3) and (8) show the lowest quality as the IVC is almost collapsed in the former one and it vanishes after the initial frames in the latter one (this is not seen in this image).

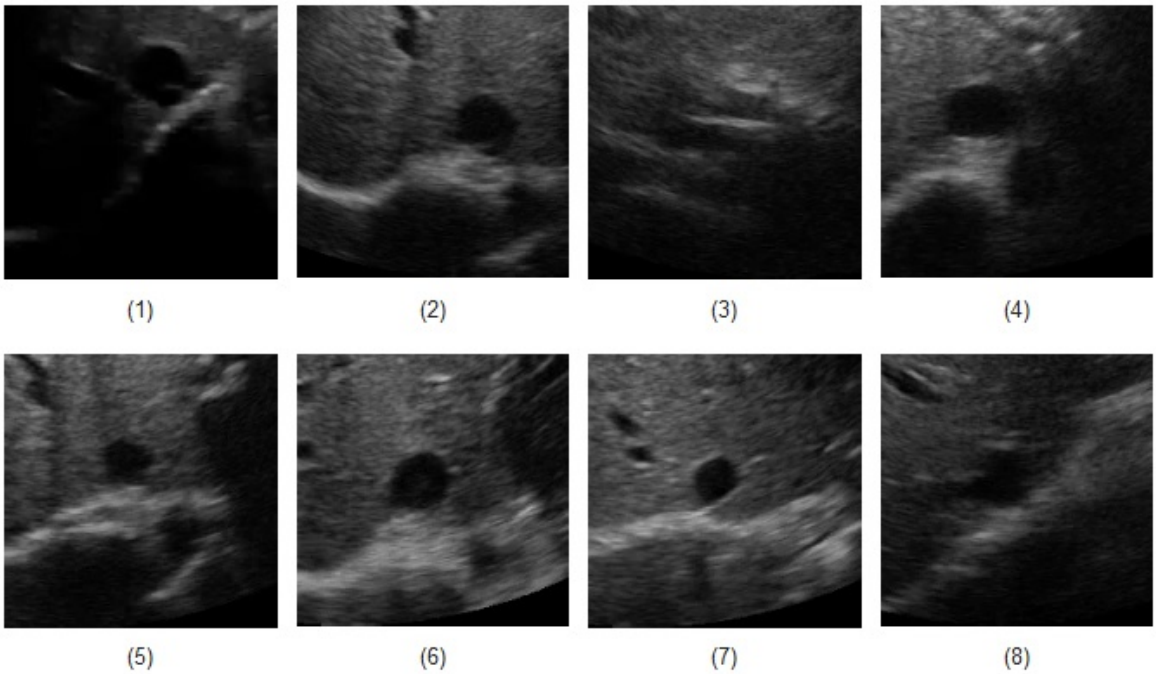

Figure 3. The first frame of the three sample IVC videos.

4.1. Tracking Performance

Figs. 4-6 present the AP-diameter manually measured by an expert and the ones that are semi-automatically estimated by the three shape-based algorithms for the three sample videos depicted as subjects (1)-(3) in Fig. 3. From Fig. 4, one can see that with the first IVC clip which has a good quality, both active circle and active rectangle algorithms efficiently track the manual measurement, although the active ellipse algorithm roughly track the manual measurement and performs poorer than the other two methods.

Fig. 5 presents the tracking results for the second clip where one can easily see that all three algorithms perform less accurate than the case in Fig. 4. This is mainly due to the fact that although the second clip seems to have a better quality than the first one, it has a more fuzzy contour, making the semi-automatic algorithms less accurate than the first clip. Similar to the first clip, we can see that the active rectangle algorithms performs better than the other two methods.

Preprints (www.preprints.org) | NOT PEER-REVIEWED | Posted: 30 October 2018 doi:10.20944/preprints201810.0704.v1

Peer-reviewed version available at J. Imaging 2019, 5, 12; doi:10.3390/jimaging5010012

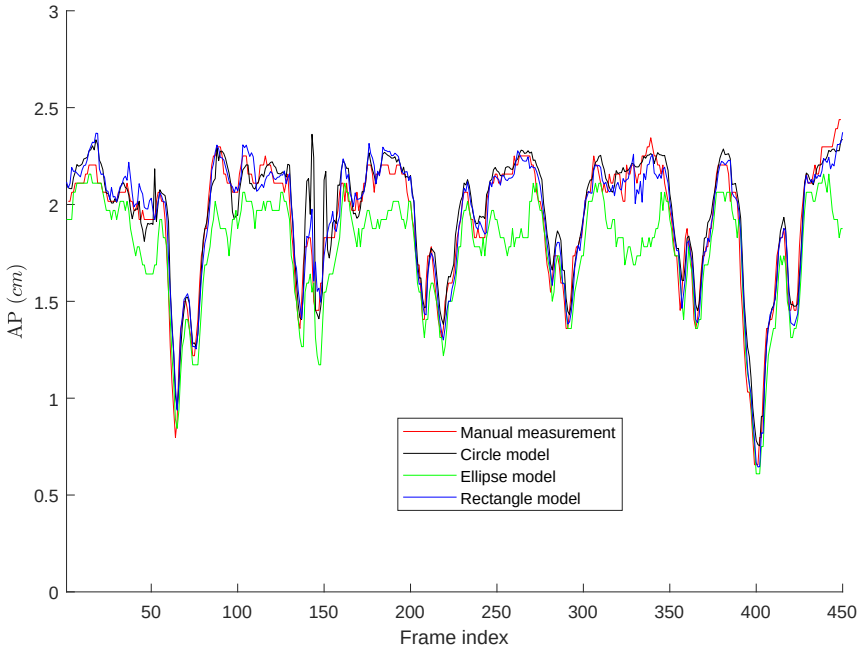

Figure 4. AP-diameter for the first sample videos depicted in Fig. 3, as measured by the manual measurement (black line), active circle algorithm (black line), active ellipse algorithm (green line) and active rectangle algorithm (blue line).

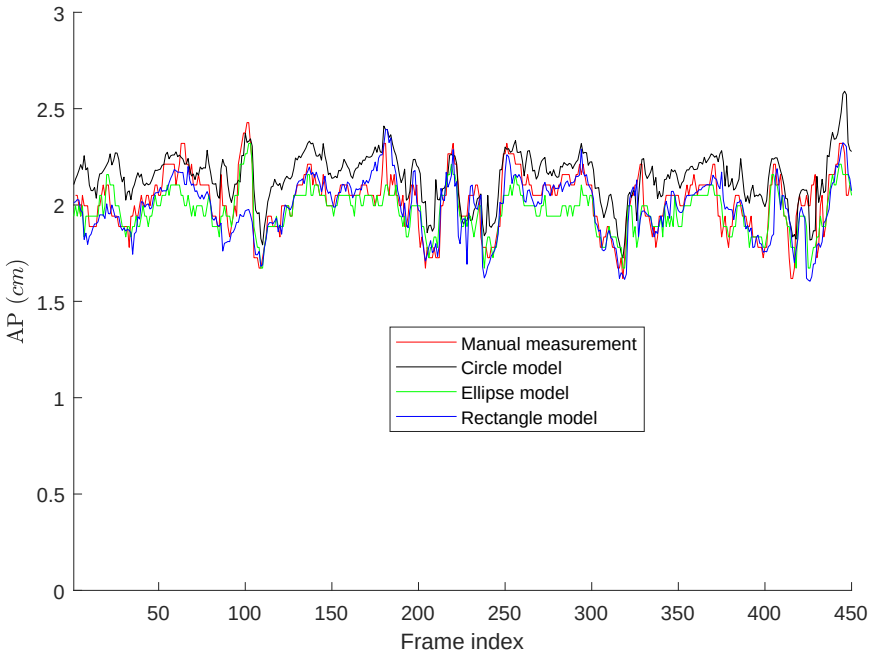

Figure 5. AP-diameter for the second sample videos depicted in Fig. 3, as measured by the manual measurement (black line), active circle algorithm (black line), active ellipse algorithm (green line) and active rectangle algorithm (blue line).

Fig. 5 presents the tracking results for the third clip depicted in Fig. 3 where the IVC is almost collapsed and therefore, a smaller AP-diameter is expected. In this case, the active circle algorithm loses the tracking after 337 frames, while both active ellipse and active rectangle algorithms efficiently track the result obtained from the manual measurement.

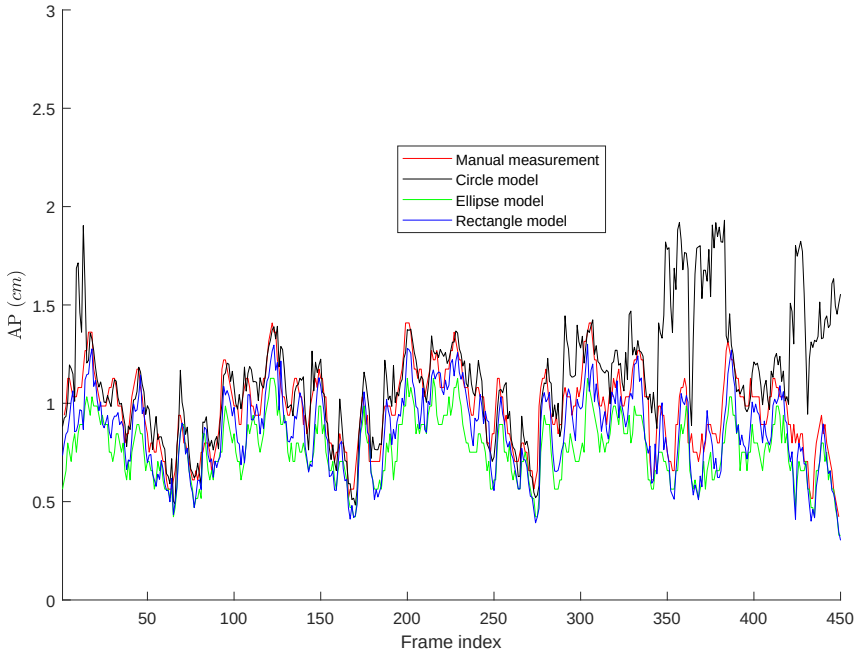

Figure 6. AP-diameter for the third sample videos depicted in Fig. 3, as measured by the manual measurement (black line), active circle algorithm (black line), active ellipse algorithm (green line) and active rectangle algorithm (blue line).

Figs. 4-6 show that in all three investigated clips, the active rectangle algorithm outperforms the other two methods. To have a better insight about the results, we present numerical results in tables 1 and 2. Table 1 present the room mean square (RMS) of the AP-diameter estimation error for the three algorithms for the all eight clips depicted in Fig. 3. Note that the error is defined as the difference between the AP-diameter estimated by each of the algorithms and the one manually measured by the expert. Except with subject no. (8), where manual segmentation is reliable for only the first 150 frames (see [23]), for the other seven subjects, the RMS of error is calculated over all 450 frames. From this table, one can see that in all eight investigated cases, the active rectangle algorithm outperforms the other two methods, while in five out of eight cases, the active circle algorithm performs more accurate than the active ellipse algorithm.

Table 2 present the maximum absolute value of error obtained for the three algorithms for all eight clips depicted in Fig. 3. This tables confirms the results obtained in Table 1, i.e., the active rectangle algorithms always outperform the other two methods.

Table 1. RMS of the AP-diameter estimation error.

Method \ Subject no.	(1)	(2)	(3)	(4)	(5)	(6)	(7)	(8)	Ave.
Circle model	0.10	0.16	0.16	0.25	0.25	0.10	0.11	0.26	0.17
Ellipse model	0.21	0.19	0.14	0.26	0.18	0.11	0.11	0.20	0.35
Rectangle model	0.08	0.11	0.12	0.23	0.14	0.10	0.10	0.18	0.12

Table 2. Maximum absolute value of AP-diameter estimation error.

Method \ Subject no.	(1)	(2)	(3)	(4)	(5)	(6)	(7)	(8)
Circle model	0.06	0.29	0.48	0.57	0.75	0.41	0.44	0.43
Ellipse model	0.11	0.32	0.35	0.59	0.48	0.54	0.47	0.38
Rectangle model	0.05	0.18	0.19	0.42	0.28	0.37	0.39	0.29

5. Discussion

5.1. The Performance of the Proposed Algorithms

As it was described earlier in the Results section, for all eight investigated clips, the active rectangle algorithm performs closer to the manual measurement than the other two methods. This is due to the fact the AP-diameter is clinically measured as the maximum diameter inside the IVC. The active circle algorithm finds the largest circle inside the IVC and assumes that the diameter of this circle can efficiently model the AP-diameter. This is technically corrected if the IVC is horizontally aligned. But based on the angle of the ultrasound prob, the IVC in the ultrasound clip can be rotated along the horizontal axis and this makes the results a little different from the clinically measured AP-diameter.

In five out of the eight cases, the active circle algorithm performed better than the active ellipse algorithm. This is mainly due to the fact that a circle has less degree of freedom compared to an ellipse and therefore, circle evolution can be performed more accurate than ellipse evolution. Furthermore, from Fig. 3, one can see that in most cases, the IVC does not appear to have an elliptical shape making the ellipse fitting process inaccurate.

5.2. Complexity Comparison

Obviously, an ellipse has five parameters to estimate while a circle has only three parameters, i.e., two for its center coordinates and one for its radius. Consequently, the active ellipse algorithm seems to be more complex than the active circle algorithm. The active rectangle algorithm also has three parameters to estimate, i.e., two for the rectangle center and one for the rectangle height, but its complexity is even much less than the active circle algorithm and it also requires less iterations to converge. Furthermore, the main source of the complexity for all these three algorithms is for computation of u and v, while with the rectangle model, u and v can be computed using the integral image which is computed only once for each frame.

6. Conclusions

In this paper, two novel algorithms based on elliptical and rectangular models were proposed for semi-automatic estimation of AP-diameter of the IVC in ultrasound videos. The proposed algorithm were compared with active circle algorithm and was shown that although IVC usually has elliptical

CSA, both circular and rectangular models provide a more accurate AP-diameter measurement, while the rectangular model outperforms both circular and elliptical models. This is due that fact that the AP-diameter is clinically measured as the maximum vertical diameter of the IVC which can be modeled better as the vertical side of a rectangle than the diameter of a circle or an ellipse.

Author Contributions: Andrew Smith provided the data and performed the manual measurement, Ebrahim Karami designed the algorithms, performed the experiments, and wrote the paper, and Mohamed Shetata and Andrew Smith edited the paper.

Conflicts of Interest: The authors declare no conflict of interest.

Abbreviations

The following abbreviations are used in this manuscript:

MDPI: Multidisciplinary Digital Publishing Institute
AP: Anterior-posterior
IVC: Inferior vena cava
CSA: Cross sectional area.

1. Smyrniotis, V.; Kostopanagiotou, G.; Theodoraki, K.; Tsantoulas, D.; Contis, J.C. The role of central venous pressure and type of vascular control in blood loss during major liver resections. *The American journal of surgery* **2004**, *187*, 398–402.
2. Rivers, E.; Nguyen, B.; Havstad, S.; Ressler, J.; Muzzin, A.; Knoblich, B.; Peterson, E.; Tomlanovich, M. Early goal-directed therapy in the treatment of severe sepsis and septic shock. *New England Journal of Medicine* **2001**, *345*, 1368–1377.
3. Charron, C.; Caille, V.; Jardin, F.; Vieillard-Baron, A. Echocardiographic measurement of fluid responsiveness. *Current opinion in critical care* **2006**, *12*, 249–254.
4. Durairaj, L.; Schmidt, G.A. Fluid therapy in resuscitated sepsis: less is more. *Chest Journal* **2008**, *133*, 252–263.
5. Barbier, C.; Loubières, Y.; Schmit, C.; Hayon, J.; Ricôme, J.L.; Jardin, F.; Vieillard-Baron, A. Respiratory changes in inferior vena cava diameter are helpful in predicting fluid responsiveness in ventilated septic patients. *Intensive care medicine* **2004**, *30*, 1740–1746.
6. Wang, W.; Zhu, L.; Qin, J.; Chui, Y.P.; Li, B.N.; Heng, P.A. Multiscale geodesic active contours for ultrasound image segmentation using speckle reducing anisotropic diffusion. *Optics and Lasers in Engineering* **2014**, *54*, 105–116.
7. Sudha, S.; Suresh, G.; Sukanesh, R. Speckle noise reduction in ultrasound images by wavelet thresholding based on weighted variance. *International journal of computer theory and engineering* **2009**, *1*, 7.
8. Wagner, R.F.; Smith, S.W.; Sandrik, J.M.; Lopez, H. Statistics of speckle in ultrasound B-scans. *IEEE transactions on sonics and ultrasonics* **1983**, *30*, 156–163.
9. Seabra, J.C.; Ciompi, F.; Pujol, O.; Mauri, J.; Radeva, P.; Sanches, J. Rayleigh mixture model for plaque characterization in intravascular ultrasound. *IEEE Transactions on Biomedical Engineering* **2011**, *58*, 1314–1324.
10. Pereyra, M.; Dobigeon, N.; Batatia, H.; Tourneret, J.Y. Segmentation of skin lesions in 2-D and 3-D ultrasound images using a spatially coherent generalized Rayleigh mixture model. *IEEE transactions on medical imaging* **2012**, *31*, 1509–1520.
11. Tuthill, T.; Sperry, R.; Parker, K. Deviations from Rayleigh statistics in ultrasonic speckle. *Ultrasonic imaging* **1988**, *10*, 81–89.
12. Karami, E.; Shehata, M.S.; Smith, A. Tracking of the Internal Jugular Vein in Ultrasound Images Using Optical Flow. The 30th Annual IEEE Canadian Conference on Electrical and Computer Engineering (CCECE), Windsor, Canada. IEEE, 2017, pp. 1–4.
13. Kass, M.; Witkin, A.; Terzopoulos, D. Snakes: Active contour models. *International journal of computer vision* **1988**, *1*, 321–331.

14. Karami, E.; Shehata, M.; McGuire, P.; Smith, A. A Semi-automated Technique for Internal Jugular Vein Segmentation in Ultrasound Images Using Active Contours. 2016 IEEE-EMBS International Conference on Biomedical and Health Informatics (BHI). IEEE, 2016, pp. 184–187.
15. Liu, B.; Cheng, H.; Huang, J.; Tian, J.; Tang, X.; Liu, J. Probability density difference-based active contour for ultrasound image segmentation. *Pattern Recognition* **2010**, *43*, 2028–2042.
16. Talebi, M.; Ayatollahi, A.; Kermani, A. Medical ultrasound image segmentation using genetic active contour. *Journal of Biomedical Science and Engineering* **2011**, *4*, 105.
17. Noble, J.A. Ultrasound image segmentation and tissue characterization. *Proceedings of the Institution of Mechanical Engineers, Part H: Journal of Engineering in Medicine* **2010**, *224*, 307–316.
18. Yim, P.J.; Foran, D.J. Volumetry of hepatic metastases in computed tomography using the watershed and active contour algorithms. Computer-Based Medical Systems, 2003. Proceedings. 16th IEEE Symposium. IEEE, 2003, pp. 329–335.
19. Ali, S.; Madabhushi, A. An integrated region-, boundary-, shape-based active contour for multiple object overlap resolution in histological imagery. *IEEE transactions on medical imaging* **2012**, *31*, 1448–1460.
20. Nakamura, K.; Tomida, M.; Ando, T.; Sen, K.; Inokuchi, R.; Kobayashi, E.; Nakajima, S.; Sakuma, I.; Yahagi, N. Cardiac variation of inferior vena cava: new concept in the evaluation of intravascular blood volume. *Journal of Medical Ultrasonics* **2013**, *40*, 205–209.
21. Baust, M.; others. Polar Active Contours for Medical Applications. PhD thesis, Technische Universität München, 2012.
22. Karami, E.; Shehata, M.; Smith, A. Segmentation and Tracking of Inferior Vena Cava in Ultrasound Images Using a Novel Polar Active Contour Algorithm. 5th IEEE Global Conference on Signal and Information Processing, GlobalSIP2017. IEEE, 2017, pp. 1–5.
23. Karami, E.; Shehata, M.; Smith, A. Estimation and Tracking of AP-diameter of the Inferior Vena Cava in Ultrasound Images Using a Novel Active Circle Algorithm. *Computers in Biology and Medicine* **2018**, *98*, 16–25.
24. Guerrero, J.; Salcudean, S.E.; McEwen, J.A.; Masri, B.A.; Nicolaou, S. Real-time vessel segmentation and tracking for ultrasound imaging applications. *IEEE transactions on medical imaging* **2007**, *26*, 1079–1090.